JACS
JOURNAL OF THE AMERICAN CHEMICAL SOCIETY
Article
pubs.acs.org/JACS

A Unique Class of Near-Infrared Functional Fluorescent Dyes with Carboxylic-Acid-Modulated Fluorescence ON/OFF Switching: Rational Design, Synthesis, Optical Properties, Theoretical Calculations, and Applications for Fluorescence Imaging in Living Animals

Lin Yuan, Weiying Lin,* Yueting Yang, and Hua Chen

State Key Laboratory of Chemo/Biosensing and Chemometrics, College of Chemistry and Chemical Engineering, Hunan University, Changsha 410082, P. R. China

Supporting Information

ABSTRACT: Fluorescence imaging is one of the most powerful techniques for monitoring biomolecules in living systems. Fluorescent sensors with absorption and emission in the near-infrared (NIR) region are favorable for biological imaging applications in living animals, as NIR light leads to minimum photodamage, deep tissue penetration, and minimum background autofluorescence interference. Herein, we have introduced a new strategy to design NIR functional dyes with the carboxylic-acid-controlled fluorescence on−off switching mechanism by the spirocyclization. Based on the design strategy, we have developed a series of Changsha (**CS1−6**) NIR fluorophores, a unique new class of NIR functional fluorescent dyes, bearing excellent photophysical properties including large absorption extinction coefficients, high fluorescence quantum yields, high brightness, good photostability, and sufficient chemical stability. Significantly, the new **CS1−6** NIR dyes are superior to the traditional rhodamine dyes with both absorption and emission in the NIR region while retaining the rhodamine-like fluorescence ON-OFF switching mechanism. In addition, we have performed quantum chemical calculations with the B3LYP exchange functional employing 6-31G* basis sets to shed light on the structure-optical properties of the new **CS1−6** NIR dyes. Furthermore, using **CS2** as a platform, we further constructed the novel NIR fluorescent TURN-ON sensor **7**, which is capable of imaging endogenously produced HClO in the living animals, demonstrating the value of our new **CS** NIR functional fluorescent dyes. We expect that the design strategy may be extended for development of a wide variety of NIR functional dyes with a suitable fluorescence-controlled mechanism for many useful applications in biological studies.

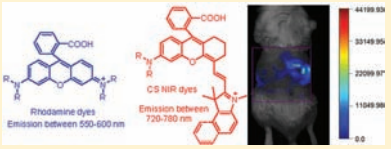

INTRODUCTION

Recently, fluorescence imaging has become one of the most powerful techniques for monitoring biomolecules in living systems.[1] Fluorescent sensors are essential molecular tools for bioimaging. So far, a large number of fluorescent sensors have been constructed.[2] However, most of them have the absorption and emission in the visible range (400−650 nm). By contrast, the fluorescent sensors with absorption and emission in the near-infrared (NIR) region (650−900 nm) are relatively few, although they are highly sought due to their useful applications in chemical biology.[1j,k,n,3] When compared to visible light, NIR light is advantageous to be employed in biological imaging due to minimum photodamage to biological samples, deep tissue penetration, and minimum interference from background autofluorescence by biomolecules in the living systems.[3]

Cyanine dyes are one type of the widely employed NIR fluorophores for NIR fluorescent sensor design. However, as pointed out by Nagano and co-workers, on−off switching of cyanine fluorescence by photoinduced electron transfer (PeT) is quite difficult, as cyanine dyes have relatively high-lying occupied molecular orbital (HOMO) energy levels.[4] Thus, the development of cyanine-based NIR sensors by means of a PeT process is very challenging.[5] In a well-designed work, Murthy's group presented a different strategy to turn on the fluorescence of cyanine-based NIR sensors with the π-electron deconjugation.[6] Very recently, Shabat et al. introduced an elegant strategy to switch on the fluorescence of cyanine-based NIR sensors by analyte-specific unmasking of a protected quinone derivative of Cy7.[7]

Rhodamine dyes have good photochemical properties such as high molar extinction coefficients, large fluorescence quantum yields, and tolerance to photobleaching.[8] Significantly, the carboxylic acid group of rhodamine dyes can undergo intramolecular cyclization (Figure 1A). The open form is highly fluorescent, whereas the spirocyclic form is essentially nonfluorescent.[8a,b] At physiological pH, the fluorescent open form is predominated. In other words, the fluorescence of rhodamine dyes is on at physiological pH. By sharp contrast, the fluorescence of rhodamine amide derivatives is off at physiological pH, as the nonfluorescent spirolactam form is predominated (Figure 1A). By exploiting the unique

Received: October 2, 2011
Published: December 15, 2011

 © 2011 American Chemical Society dx.doi.org/10.1021/ja209292b | J. Am. Chem.Soc. 2012, 134, 1200−1211

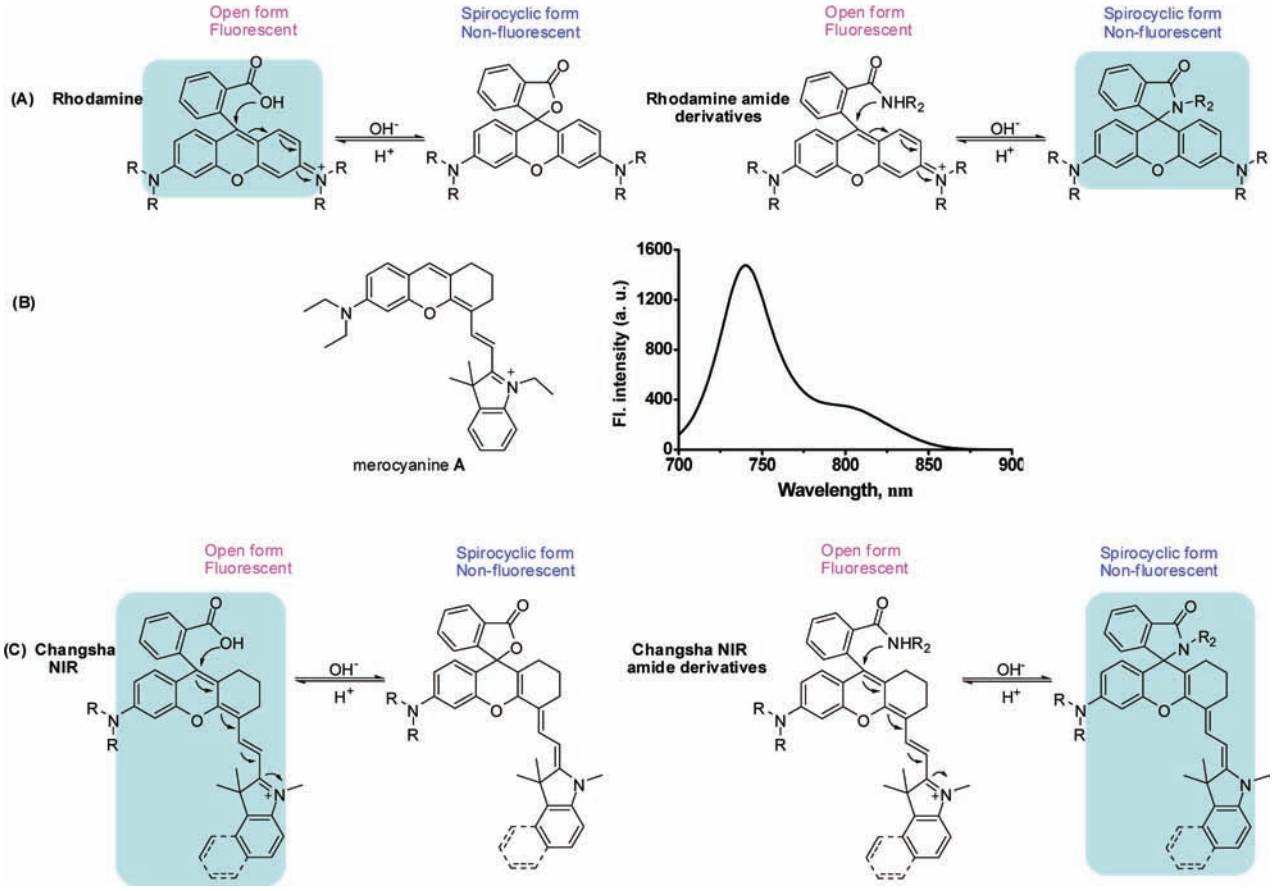

Figure 1. Design strategy for the new Changsha (**CS**) NIR functional dyes with a rhodamine-like carboxylic-acid-modulated fluorescence on/off switching mechanism. (A) Spirocyclization of the classic rhodamine and rhodamine amide derivatives. (B) Structure and the fluorescence emission spectrum (in CH_3OH) of merocyanine dye **A**. Notably, the emission profile of merocyanine dye **A** has not been previously disclosed. (C) Spirocyclization of the new Changsha (**CS**) and Changsha amide derivatives. The highlighted structures are the putative forms predominantly present at physiological pH. Significantly, the electronic pulling pathway for the novel **CS** NIR functional dye spirocyclization highly resembles that of the traditional rhodamine dye spirocyclization.

fluorescence ON−OFF switching between rhodamine dyes and their amide derivatives, in a pioneering work, Czarnik's group constructed a fluorescence turn-on sensor for copper ions.[9] The specific copper-mediated hydrolysis of nonfluorescent rhodamine B hydrazide into fluorescent rhodamine B was employed in this case. Since then, the rhodamine spirolactam has been employed as an effective platform for construction of fluorescence turn-on sensors for a diverse array of targets including Cu^{2+}, Hg^{2+}, Fe^{3+}, Cr^{3+}, Pb^{2+}, Zn^{2+}, Ag^{+}, Au^{3+}, Pd^{2+}, Pt^{2+}, HOCl, and NO, based on the unique spirolactam ring-opening process of rhodamines.[8a,b,10] Thus, the rhodamine spirolactam platform is one of the most robust platform for fluorescent sensor development. However, the fluorescence turn-on sensors derived from the classic rhodamine dyes such as rhodamine B, rhodamine 6G, and rhodamine 101 have absorption and emission only in the visible region (500−600 nm). This limitation renders them unsuitable for biological imaging in living animals. Thus, it is highly desirable to develop rhodamine analogues with absorption and emission in the NIR region.

In this regard, some NIR rhodamine analogues have been constructed.[11] For example, rhodamine 800 (Abs_{max}/Em_{max} = 680/700 nm) is commercially available (The structure is shown in Figure S1). However, it has a CN functional group instead of benzoic acid at the 9-position of rhodamine. Thus, rhodamine 800 lacks the unique spirolactone ring-opening process of rhodamines. In other words, the fluorescence on−off switching of rhodamine 800 cannot be readily achieved by the interconversion between the fluorescent open form and the nonfluorescent spirocyclic form. Thus, rhodamine 800 is only suitable as NIR fluorescent labels for biomolecules, but not as the platform for design of analyte-responsive NIR fluorescent sensors. Recently, in an elegant work, Nagano et al. developed a Si-rhodamine-based[12a] fluorescent hypochlorous acid sensor with absorption and emission located in the far-red to near-infrared region (Abs_{max}/Em_{max} = 652/670 nm), and it operates by the typical spirocyclization-based fluorescence on−off switching mechanism.[12b] The red-shift of Si-rhodamine derivatives compared to the classic rhodamine dyes is believed due to the relatively low lying LUMO energy levels of silicon. However, to obtain rhodamine analogues with longer absorption and emission (>700 nm) while retaining the unique spirocyclization-based fluorescence on−off switching mechanism of rhodamines, a distinct novel strategy is needed to modify rhodamine dyes. This appears to be a challenging but interesting task.

It has been reported that merocyanine **A** (Figure 1B) has maximal absorption at around 700 nm, in the NIR region.[13] However, to the best of our knowledge, the fluorescence properties of merocyanine **A** have not been reported in the

dx.doi.org/10.1021/ja209292b | J. Am. Chem.Soc. 2012, 134, 1200−1211

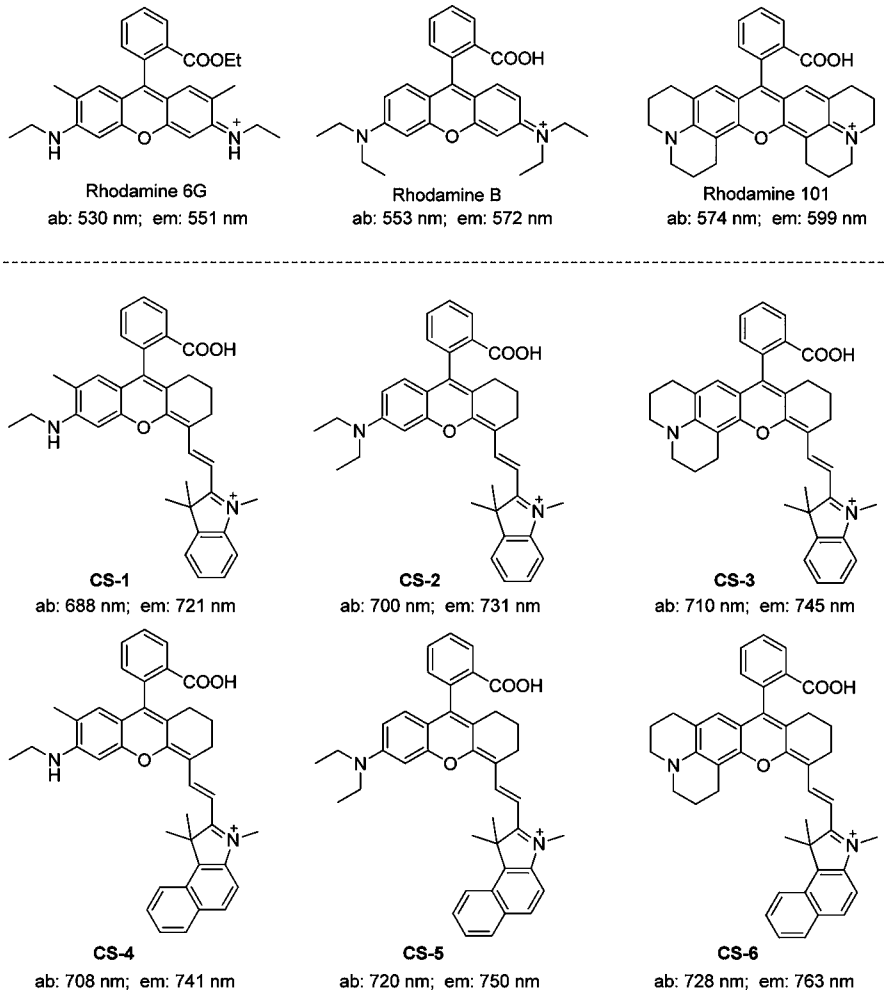

Figure 2. Comparison of the classical rhodamine dyes and the novel **CS** NIR dyes. Top: Structures of the classical rhodamine dyes (rhodamines B, 6G, 101). Bottom: Structures of the newly designed NIR dyes **CS1−6**.

literature. Thus, we decided to synthesize and examine the fluorescence profiles of merocyanine **A**. Our studies reveal that merocyanine **A** has a strong emission peak at 734 nm (Figure 1B) with a high fluorescence quantum yield of 0.34 in CH_3OH. Obviously, it is difficult to control the optical properties of merocyanine **A**, as it lacks of a simple fluorescence switching mechanism. However, we envisioned that merocyanine **A** could be employed as a building block to design new NIR fluorescent platforms with tunable optical properties, if a handy fluorescence switching mechanism can be rationally installed.

Toward this end, in this work, based on the above design strategy, we have developed a new type of NIR functional dyes, called Changsha (**CS**) NIR, which is the hybrid of merocyanine **A** and benzoic acid (Figure 1C). In principle, the merocyanine **A** unit could show the desired NIR optical profiles. We further hypothesized that the carboxylic acid functional group could operate as a fluorescence on−off switcher by spirocyclization. In other words, the novel **CS** NIR dyes may bear the same robust fluorescence ON−OFF switching mechanism as the traditional rhodamine dyes (Figure 1A) while having the advantage of NIR absorption and emission, as the driving force for the spirocyclization of the new **CS** NIR dyes and the traditional rhodamine dyes is quite similar, an iminium moiety (notably, the electronic pulling pathway for the **CS** NIR dye spirocyclization highly resembles that of the traditional rhodamine dye spirocyclization; see Figure 1A and C). Since **CS** NIR dyes intrinsically bear a handy fluorescence on−off switching mechanism, they could serve as the effective new platforms for NIR fluorescent sensor design. Herein, we described the design, synthesis, and optical properties of the new class of **CS** NIR functional dyes. To get insight into the structure−optical properties of the **CS** NIR functional dyes, we further performed quantum chemical calculations with the B3LYP exchange functional employing 6-31G* basis sets using a suite of Gaussian 09 programs. Furthermore, based on a novel **CS** NIR platform, we constructed a new NIR fluorescent TURN-ON sensor, which is suitable for fluorescence imaging of endogenously produced HClO in the living animals.

■ RESULTS AND DISCUSSION

Design and Synthesis of a Series of Changsha NIR Dyes (CS1−6). It is known that the absorption and emission wavelengths of traditional rhodamine dyes are highly dependent on the substituents on the amino group. For instance, rhodamines 6G, B, and 101 emit at 551, 572, and 599 nm, respectively.[8] To provide a series of Changsha NIR dyes with diverse absorption and emission wavelengths, we first designed NIR dyes **CS 1−3** (Figure 2), in parallel to rhodamines 6G, B, and 101. On the other hand, it is known that the absorption and emission wavelengths of traditional cyanine dyes could be tuned with distinct substituents on the indolium moiety. It has

dx.doi.org/10.1021/ja209292b | J. Am. Chem.Soc. 2012, 134, 1200−1211

Scheme 1. Synthesis of NIR Dyes CS1−6[a]

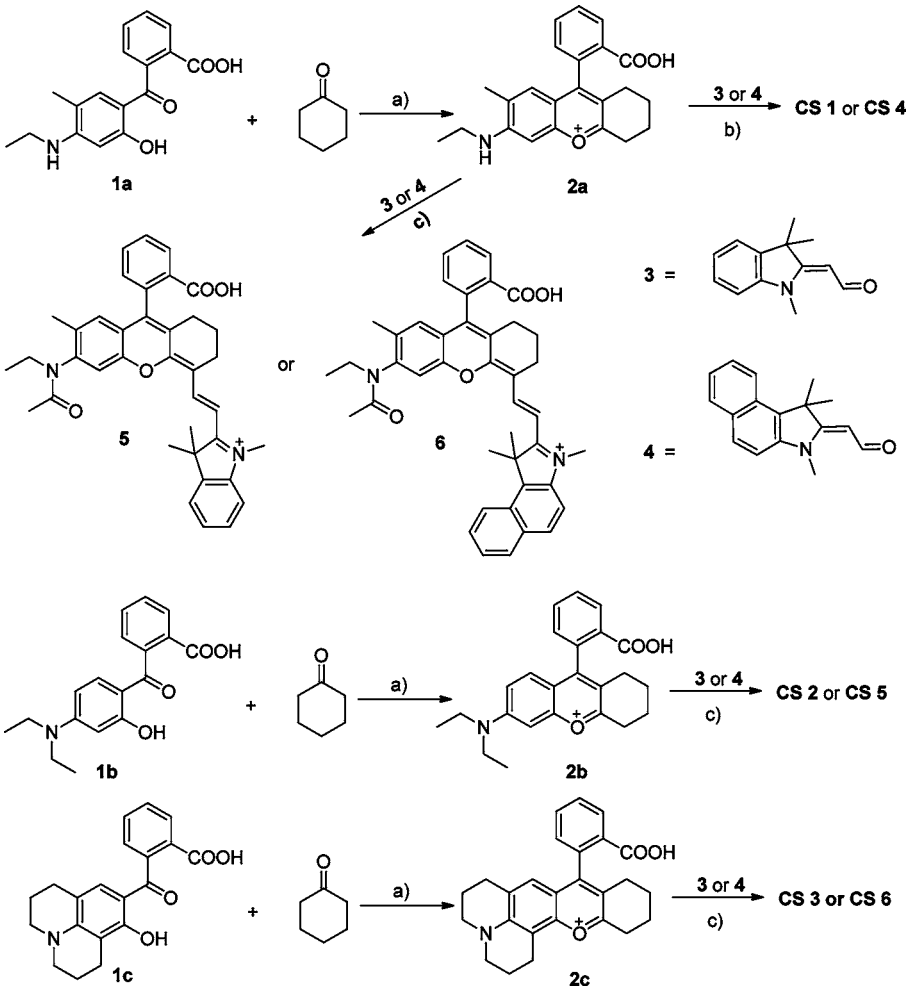

[a]Conditions: (a) H_2SO_4, Δ, then 70% $HClO_4$; (b) acetic anhydride, 25 °C, 10 min; (c) acetic anhydride, 50 °C, 30 min.

been reported that benzo[e]indole-based cyanines have a bathochromic shift of 20 nm when compared to indole-based cyanines.[14] On the basis of this consideration, we further designed **CS 4−6** to bear the benzo[e]indole moiety, in parallel to **CS 1−3**. We anticipated that **CS 4−6** may have longer absorption and emission wavelengths relative to the corresponding NIR dyes **CS 1−3**. Overall, we should have six new NIR dyes, **CS 1−6**, with diverse wavelengths in the NIR region.

A retrosynthesis analysis of compounds **CS1−6** is shown in Scheme S1. Based on the proposed retrosynthesis analysis, we designed a facile synthetic route to **CS1−6** as outlined in Scheme 1. Fisher aldehyde **3** is commercially available, and the starting materials **1a−c** and **4** were prepared according to the reported procedures.[10h,15,16] Condensation of compound **1a** with cyclohexanone in acidic conditions afforded the critical intermediate **2a**, which was then condensated with aldehyde **3** or **4** under very mild conditions (in acetic anhydride at 25 °C within 10 min) to give the product **CS1** or **CS4** as a bright green solid, respectively. The key to obtain the desired product **CS1** or **CS4** is to control the reaction time (less than 10 min), as prolonged reaction time would lead to the formation of byproduct **5** or **6**, the acetylated derivatives of **CS1** or **CS4**. We reasoned that this is due to the solvent of the reaction, acetic anhydride, which is a good acetylating reagent and could further react with the ethylamino group of **CS1** or **CS4** at the prolonged reaction time. The similar synthetic pathway was employed to synthesize compounds **CS2**, **CS3**, **CS5**, and **CS6**. Since the additional acetylation is not impossible, the synthesis of **CS2**, **CS3**, **CS5**, and **CS6** proceeded at 50 °C for 30 min in acetic anhydride for a good yield. Although compounds **5** and **6** are not the desired products, we envisioned that they could serve as the control compounds in the process of the examination of the structure-optical properties of **CS1−6**. The structures of the products **CS1−6** and controls **5**, **6** were fully characterized by ^{1}H NMR, ^{13}C NMR, MS (ESI), and HRMS (ESI). Notably, the modular nature of the synthetic strategy may allow it to be adapted to prepare a wide variety of Changsha (**CS**)-type of NIR fluorescent dyes bearing distinct substituents on the amino group and the indolium moieties. Furthermore, the synthetic strategy is facile and scalable for production of the new NIR dyes in large quantity.

Optical Properties. The absorption and emission profiles of compounds **CS1−6** in distinct solvents (EtOH, MeOH, CH_3CN, pH 7.4 PBS/CH_3OH (v/v, 8: 2), $CHCl_3$) are shown in Figures 3 and S2−5, and the corresponding photophysical data are compiled in Tables 1 and S1−4, respectively. As designed, in general, compounds **CS1−6** display both absorption and emission peaks well into the NIR region, with maximum at 688−728 nm and 721−763 nm in EtOH, respectively (Table 1). Interestingly, **CS1−6** tend to exhibit

dx.doi.org/10.1021/ja209292b | J. Am. Chem.Soc. 2012, 134, 1200−1211

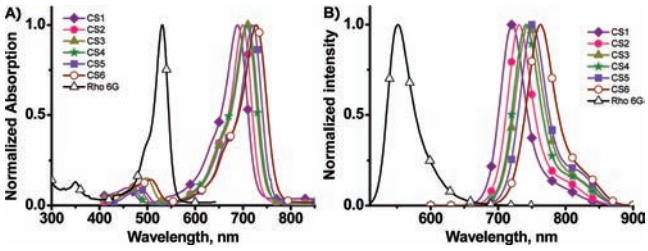

Figure 3. Absorption (A) and emission (B) spectra of compounds **CS1** (dark purple tilted square), **CS2** (magenta circle), **CS3** (olive-green triangle), **CS4** (green star), **CS5** (purple square), and **CS6** (maroon open circle) in EtOH. For comparison, the absorption and emission spectra of rhodamine 6G (black open triangle) are also shown.

longer absorption and emission in CH_3CN. For instance, **CS6** has an emission peak with maximum at 780 nm (Table S2), which further extends to 870 nm in CH_3CN (Figure S3B). Thus, the emission of **CS1−6** covers a significant part of the "biological window (650−900 nm)" for in vivo imaging, indicating the potential use of these new NIR dyes for biological imaging in living animals.

CS1 shows an intense absorption band with maximum at 688 nm, assigned to the 0−0 band of the S1←S0 transition, and a (less pronounced) shoulder peak on the high-energy side (at around 650 nm), attributed to the 0−1 vibrational band of the same transition (Figure 3A). In addition, **CS1** also bears a very weak and broad absorption band at around 460 nm, which can be attributed to the S3←S0 transition. Close examination reveals that the shape of the absorption spectrum of **CS1** is highly resemble to that of rhodamine 6G, indicating that **CS1** may be called the analogue of rhodamine 6G at some sense. However, significantly, **CS1** displays a striking advantage over rhodamine 6G: The absorption of **CS1** has a large red-shift (160 nm) in comparison to rhodamine 6G (Figure 3A). For the emission, as shown in Figure 3B, **CS1** has an intense emission peak with maximum at 721 nm, extending to 850 nm. In good agreement with the findings in the absorption, **CS1** also exhibits a drastic bathochromic shift (160 nm) in emission while maintaining the similar shape in the emission spectrum when compared to rhodamine 6G. The same red-shift trend was observed in **CS2** and **CS3** relative to rhodamines B and 101, respectively, validating the design strategy. On the other hand, the emission wavelengths of these new NIR functional dyes are in the order of **CS3** > **CS2** > **CS1**, and the same order was observed for the corresponding rhodamines (rhodamine 101 > rhodamine B > rhodamine 6G),[8] further corroborating our design strategy. As anticipated, the emission bands of **CS4**, **CS5**, and **CS6** peak at 741, 750, and 763 nm, respectively, which have an around 20 nm red-shift when compared to the corresponding **CS1**, **CS2**, and **CS3**. This bathochromic shift behavior is consistent with that observed for benzo[e]indole-based cyanines over indole-based cyanines.[14]

The molar extinction coefficients (ε_{max}) of the new NIR dyes **CS1−6** are in the range of 110 000 −140000 $M^{-1}cm^{-1}$, which are superior or comparable to those of the classic rhodamine dyes (80 000−120 000 M^{-1} cm^{-1}). Remarkably, **CS1−6** have the fluorescence quantum yields (Φ_f) of 0.29−0.56 in EtOH, which are great values for NIR functional dyes. In addition, the brightness ($\varepsilon_{max}\Phi_f$) of **CS1−6** is in the range of 37 816−73 640 M^{-1} cm^{-1}, which is comparable or superior to those of the classic rhodamine dyes (for example, rhodamine B (52 650 M^{-1} cm^{-1}) in EtOH.[8b] Furthermore, the Stokes shifts of **CS1−6** are from 31 to 35 nm, comparable to those of the typical rhodamine and cyanine dyes.

We then examined the fluorescence profiles of the new dyes and their amide derivatives at different pH values. As a representative example, **CS 2** (Figure 4A) and its amide derivative **CS2-NH_2NH_2** (Figure 4B) were studied. As shown in Figure 4C, **CS 2** is highly fluorescent over a wide pH range of 5−11. However, the fluorescence drops significantly at higher pH values (>11) likely due to the formation of the nonfluorescent spirocyclic form (Figure 4A). pK_{cycl} denotes the pH value at which the emission of the compound decreases to half the maximum emission due to the spirocyclization.[1m] The pK_{cycl} of **CS 2** was determined to be over 12. In sharp contrast, **CS2-NH_2NH_2**, the amide derivative of **CS 2**, has a pK_{cycl} of 4.3 (Figure 4B). These results indicate that, at the physiological pH of ∼7.4, **CS 2** is present mainly as the fluorescent open form, while **CS2-NH_2NH_2** predominately exists as the nonfluorescent spirocyclic form. In other words, the fluorescence of **CS2** is on while its amide derivative **CS2-NH_2NH_2** is off at physiological pH. The fluorescence on−off switching of **CS** dyes and their amide derivatives is very similar to that of the classic rhodamines and their amide derivatives. This implies that, like the classic rhodamines,[8a,b,9,10] the new **CS** NIR dyes could be utilized as platforms to design NIR fluorescent sensors.

It is of importance to evaluate both the photostability and chemical stability of functional fluorescent dyes intended for bioapplications. The photostability of **CS1−6** in EtOH solution

Table 1. Photophysical Data of the Dyes CS1−6, 5, and 6, Rhodamines 6G, B, and 101 in EtOH

dye	λ_{abs}/nm[a]	ε_{max}/M^{-1} cm^{-1}	λ_{em}/nm[b]	Φ_f[c]	Stokes shift	fwhm/nm[d]
CS 1	688	131 500	721	0.56	32	43
CS 2	700	139 500	731	0.41	31	42
CS 3	710	125 445	745	0.34	35	48
CS 4	708	135 880	741	0.34	33	45
CS 5	720	125 971	750	0.30	30	44
CS 6	728	130 400	763	0.29	35	48
5	612/656	54 120/49 913	687	<0.005	75/31	90
6	632/678	55071/43618	715	<0.005	83/37	90
Rho 6G	530	116 000	551	0.95[8c]	21	
Rho B[8b]	553	117 000	572	0.53	19	
Rho 101[8b]	574	110 000	599	0.89	25	

[a]The maximal absorption of the dye. [b]The maximal emission of the dye. [c]Φ_f is the relative fluorescence quantum yield estimated by using ICG (Φ_f = 0.13 in DMSO) as a fluorescence standard.[17,18] [d]The full width at half-maximum height.

dx.doi.org/10.1021/ja209292b | J. Am. Chem.Soc. 2012, 134, 1200−1211

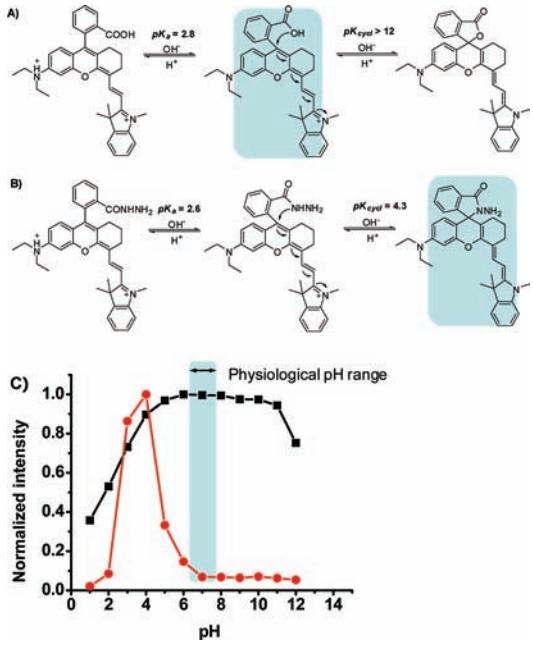

Figure 4. (A,B) Structures of (A) **CS2** and (B) **CS2-NH_2NH_2** mainly present at various pH values. The highlighted structures are the putative forms predominantly present at the physiological pH. (C) pH-dependence of the fluorescence intensity of **CS2** (black square) and **CS2-NH_2NH_2** (red circle).

was measured by continuous irradiation with a Xe lamp (150 W) at 10 nm slit width at the maximal absorption wavelength of **CS1−6**, and the results demonstrate that over 97% of the initial fluorescence intensity was retained after 1 h irradiation (Figure S8A), indicating that these novel functional NIR dyes have sufficient photostability for potential biological applications. It is known that many long wavelength organic dyes are easily bleached by various oxidants.[17] Thus, we decided to investigate the emission profiles of the new **CS** NIR dyes in the presence of biologically relevant oxidants, reactive oxygen species (ROS). As a representative case, **CS2** was treated with 100 μM hydroxyl radical (OH·), H_2O_2, HClO, *tert*-butyl hydroperoxide (TBHP), and *tert*-butoxy radical (·O*t*Bu) for 30 min. As demonstrated in Figure S8B, the emission profile of **CS2** is almost unchanged. Furthermore, over 94% of the initial fluorescence intensity was still retained after treatment of **CS2** with HClO (a biologically significant ROS) for 70 min (Figure S8C). Thus, these data suggest that the new functional NIR dyes have sufficient chemical stability.

We also investigated the optical properties of controls **5** and **6**, the acetylated derivatives of compounds **CS1** and **CS4**, respectively. However, the optical profiles of controls **5** and **6** (Figure S9) are drastically distinct from those of **CS1** and **CS4**. Controls **5** and **6** have very broad and blue-shifted peaks in the absorption ranging from 500 to 700 nm. By contrast, the absorption bands of **CS1** and **CS4** are relatively sharp in the NIR region. In addition, controls **5** and **6** are almost nonfluorescent with fluorescent quantum yields < 0.005, whereas **CS1** and **CS4** are highly fluorescent with large fluorescent quantum yields up to 0.56. The dramatic distinction in the optical profiles of **5** and **6** relative to **CS1** and **CS4** can be attributed to the acetyl group on the nitrogen atom, which significantly diminishes the electron donating ability of the nitrogen atom. The similar behavior was observed on the classic rhodamines or its analogues.[19] We further performed quantum chemical calculations with the B3LYP exchange functional employing 6-31G* basis sets using a suite of Gaussian 09 programs to get insight into this phenomenon (see below). Although controls **5** and **6** are essentially nonfluorescent, we envisioned that they can be employed as"latent" fluorophores for potential applications in chemical biology.[19a,b]

Thus, the above optical studies indicate that the new functional NIR dyes **CS1−6** have the important parameters such as molar absorptivity, quantum yields, Stokes shifts, and brightness superior to or comparable to those of the classic rhodamine dyes. In addition, **CS1−6** possess good photostability and chemical stability. Interestingly, the shape of both absorption and emission spectra of **CS1−6** highly resembles that of the classic rhodamine dyes. Significantly, like the classic rhodamine dyes, **CS1−6** also intrinsically bear a carboxylic-acid-controlled fluorescence on−off switching mechanism, as they have very similar electron pulling systems for spirocyclization. However, notably, new functional NIR dyes **CS1−6** are advantageous over the classic rhodamine dyes, as **CS1−6** have both absorption and emission in the NIR region (in some case, extending up to 870 nm). Thus, novel NIR dyes **CS1−6** may have the potential as the NIR surrogates of the classic rhodamine dyes with promising biological imaging applications in living animals.

Density Functional Theory (DFT) Calculations. To shed light on the optical properties of new functional NIR fluorescent dyes **CS1−6** and controls **5** and **6**, DFT calculations with the B3LYP exchange functional employing 6-31G* basis sets using a suite of Gaussian 09 programs[20] were conducted. Figures 5 and S10−14 show the representative optimized

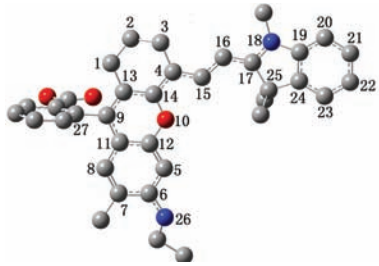

Figure 5. DFT optimized structure of **CS 1**. In the ball-and-stick representation, carbon, nitrogen, and oxygen atoms are colored in gray, blue, and red, respectively. H atoms were omitted for clarity.

structures of **CS1−6**. The C−C (N or O) bond lengths (in pm) of **CS1−6** determined by DFT calculations are displayed in Tables 2 and S5−9, and the HOMO/LUMO molecular orbital plots of **CS1−6** and controls **5** and **6** are exhibited in Figure 6. In the case of **CS1**, the benzoic acid moiety is highly twisted and essentially vertical to the 2,3-dihydro-1H-xanthene core with a dihedral angle of 89.8° (Figure 5). The C9−C27 length is 149.8 pm (Table 2), which is close to the typical carbon−carbon single bond (154 pm). These findings reveal that the benzoic acid moiety and the 2,3-dihydro-1H-xanthene core are essentially electronically decoupled. In other words, they are orthogonal and almost no electronic conjugation, in good agreement with the observation that the benzoic acid unit has essentially no contribution to the HOMO/LUMO of **CS1** (Figure 6). Interestingly, this finding is highly resemble to the case in the classic xanthene-based fluorophores (i.e., fluorescein), in which the benzoic acid moiety and the xanthene core are electronically decoupled.[21] On the other

dx.doi.org/10.1021/ja209292b | *J. Am. Chem.Soc.* 2012, 134, 1200−1211

Table 2. Representative C−C (N or O) Bond Lengths (in pm) of CS 1 Determined by DFT Calculations

C−C bond	bond lengths (in pm)	C−C bond	bond lengths (in pm)	C−C bond	bond lengths (in pm)	C−N/O bond	bond lengths (in pm)
C5−C6	140.9	C11−C12	140.9	C4−C15	139.3	C14−O10	135.9
C6−C7	142.9	C11−C9	142.8	C15−C16	140.5	O10−C12	136.4
C7−C8	138.9	C9−C13	139.1	C16−C17	139.1	C6−N26	136.7
C8−C11	141.4	C13−C14	141.9			C17−N18	136.2
C5−C12	138.9	C14−C4	141.8	C9−C27	149.8	N18−C19	141.5

hand, the indolium moiety is coplanar and perfectly conjugated with the 2,3-dihydro-1H-xanthene core. Notably, all the C−C bond lengths of the conjugated 2,3-dihydro-1H-xanthene-indolium backbone are very similar, at around 140 pm (Table 2). This value is the intermediate between the typical carbon−carbon single (154 pm) and double (134 pm) bonds, attributed to the strong electronic delocalization and the partial decrease in the carbon−carbon bond length alternation (BLA, difference between consecutive single and double bonds) along the π-conjugated system.[22] This is further confirmed by the analysis of the terminal C−N and C−O bond lengths in the conjugated system. The bond lengths of C6−N26 and C17−N18 are 136.7 and 136.2 pm, respectively, which are the intermediates between the lengths of C−N bond (single bond, around 147 pm) and the iminium C═N (double bond, around 128 pm). The bond lengths of C14−O10 and O10−C12 are 135.9 and 136.4 pm, respectively, which are the intermediates between the lengths of C−O (single bond, around 144 pm) and C═O (double bond, around 121 pm). Significantly, these results are in accordance with the absorption spectrum of **CS 1** (Figure 3A), which bears a sharp and intense absorption band in the NIR spectral range resulting from the reduced vibronic contribution in the nonalternating structure, a characteristic of cyanine dyes in the "*cyanine limit*".[22] In addition, time-dependent DFT (TDDFT) calculations indicate that **CS1** has a strong absorption band at long wavelength (f(oscillator strength) = 1.275) attributed to the S1←S0 transition and a weak absorption band at short wavelength (f = 0.435) assigned to the S3←S0 transition. Thus, the results of TDDFT calculations are in good agreement with the absorption spectra of **CS1** observed experimentally (Figure 3A).

The π electrons on the HOMO of **CS1** is mainly located on the whole π-conjugated 2,3-dihydro-1H-xanthene-indolium framework (including the amino group), but the LUMO is mostly positioned at the center of the conjugated 2,3-dihydro-1H-xanthene-vinyl bridge (Figure 6), where the BLA is minimal. When the substituent on the amino group was changed from monoethylamino (**CS1**), diethylamino (**CS2**), to fused amino (**CS3**), the energy levels of both HOMO and LUMO increase relative to those of **CS1** due to the enhanced hyperconjugation between the electrons in the σ bonds of the substituents on the amino group with the adjacent p and π orbitals, giving an extended molecular orbital which boosts the stability of the system (Figure 6). However, the HOMO energy level raises more pronouncedly than the LUMO level. Thus, the HOMO−LUMO energy gaps of **CS2** and **CS3** become smaller relative to that of **CS1**. The HOMO−LUMO energy gaps of these new functional NIR dyes obey the following order: **CS1** > **CS2** > **CS3**, which is in good agreement with the measured emission wavelengths of them, in the order of **CS1** < **CS2** < **CS3**.

The HOMO−LUMO energy gaps and the emission wavelengths of **CS4−6** are also closely correlated. The N18−C19 bond length (141.4 pm) of **CS4** is much longer than that

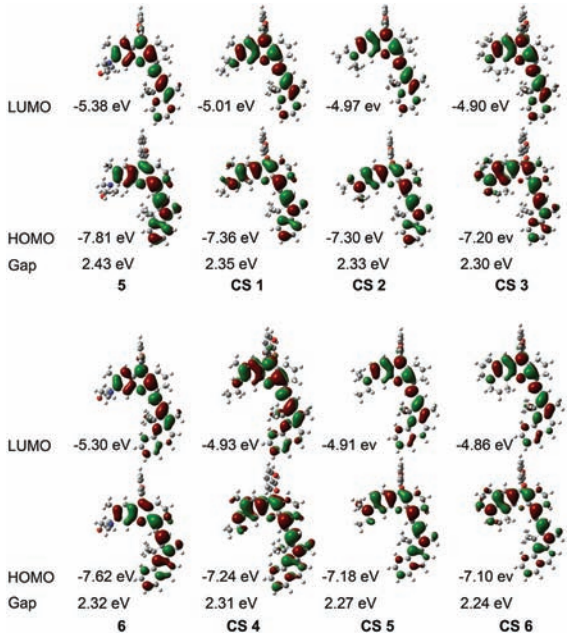

Figure 6. Molecular orbital plots (LUMO and HOMO) and HOMO/LUMO energy gaps of NIR dyes **CS1−6** and controls **5** and **6**.

of C17−N18 (135.9 pm) (Table S7), and the electrons in the fused phenyl moiety only have minor contributions to the HOMO of **CS4** (Figure 6). These data could account for only a moderate enhancement of the energy levels of both HOMO and LUMO of **CS4** in comparison to those of **CS1**. However, the HOMO level increases more markedly than the LUMO level. Thus, the HOMO−LUMO gap of **CS4** is smaller than that of **CS1**, consistent with the observation that the emission wavelength of **CS4** has a slight red-shift (20 nm) compared to **CS1**. The similar findings are present in **CS5** and **CS6** relative to **CS2** and **CS3**.

From the structure point of view, the only difference between control **5** and **CS1** is that there is an acetyl group on N26. However, this subtle distinction apparently elicits a significant effect on the molecular structures, which may account for their drastic difference in the optical properties. The C6−N26 bond length of compound **5** is 142.4 pm (Figure S15, Table S10), which is longer than that (136.7 pm) of C6−N26 of **CS1** and that (135.6 pm) of C17−N18 of compound **5**. This weakens the p−π conjugation between the amino group and π-conjugated xanthene−indolium framework, and the energy levels of both HOMO and LUMO decrease relative to those of **CS1** (Figure 6). Close examination reveals that the π electrons on the HOMO of control **5** are mainly located on the π-conjugated xanthene−indolium framework, while the lone pair electrons of N26 no longer contributes to the HOMO of compound **5**. By contrast, the lone pair electrons of N26 contribute to the HOMO of **CS 1**. This suggests that the acetylation on N26 atom indeed decreases the electron-

dx.doi.org/10.1021/ja209292b | *J. Am. Chem.Soc.* 2012, 134, 1200−1211

donating ability of the nitrogen atom, and compound **5** loses its "*cyanine limit*" structure to some extent. In other words, the acetylation on N26 atom forbids the formation of the resonance form. This could account for the blue-shift in fluorescence and much lower quantum yield of control **5** compared to **CS1**. In addition, the observation that **CS 2** and **CS2-NH$_2$NH$_2$** have low fluorescence at strong acidic conditions could also be explained by the protonation of the nitrogen atom (Figure 4), which significantly diminishes the electron donating ability of the nitrogen atom. Raines et al. pointed out that the decrease of electron-donation capability of the different nitrogen substituents of the classic rhodamines contributes to the reduction in quantum yields by decreasing the C−N bond order and thus enhancing nonradiative decay of the excited state through vibrational relaxation processes.[19a] Thus, our findings in new **CS** NIR dyes are in good agreement with those in the classic rhodamines. The drastic distinction between the optical properties of control **6** (Figure S16, Table S11) and **CS4** can be explained in a similar manner.

Development of a Novel NIR Fluorescent Turn-on HClO Sensor and Its Application for Biological Imaging in the Living Animals. New NIR functional fluorescent dyes **CS1−6** bear excellent photochemical properties including large absorption extinction coefficients, high fluorescence quantum yields, high brightness, sufficient photostability and chemical stability, and, most importantly, both absorption and emission in the NIR region. These desirable features should render the novel NIR functional fluorescent dyes suitable for fluorescence staining in the living animals. To demonstrate this possibility, as a representative example, the new NIR functional fluorescent dye **CS2** was injected into the living mice, and a large fluorescence signal was noted within a few minutes of injection (Figure S17). This indicates the potential in vivo imaging applications of the new NIR dyes.

Notably, another important character of the unique NIR functional dyes **CS1−6** is that, like classic rhodamines, they have the carboxylic-acid-regulated fluorescence on−off switching mechanism by the spirocyclization. This implies that, like classic rhodamines, **CS1−6** could be employed as robust platforms for development of NIR fluorescent sensors for biological imaging applications in living animals.

Toward this end, we constructed a novel NIR fluorescent turn-on sensor **7** (Scheme 2) for biological imaging of endogenously produced HClO in both the living macrophage cells and the living mice. Reactive oxygen species (ROS) mediate a wide variety of biological processes in the healthy and disease states. Hypochlorous acid (HOCl), one of the biologically significant ROS, is produced from peroxidation of chloride ions catalyzed by the enzyme myeloperoxidase (MPO) in activated leukocytes.[23] However, abnormal levels of HOCl are implicated with many inflammation-associated diseases including cardiovascular diseases, rheumatoid arthritis, and cancer.[24] Thus, the detection of endogenously produced HClO in living systems is very important. Briefly, the design of NIR fluorescent turn-on sensor **7** was based on the oxidant-mediated reaction of thiosemicarbazides to 1,3,4-oxadiazoles.[25] We hypothesized that the thiosemicarbazide-based **7** is nonfluorescent as the spirocyclic form is predominated at physiological pH. However, upon reaction with HClO, the thiosemicarbazide should be converted to 1,3,4-oxadiazole (Scheme S2). The resulting 1,3,4-oxadiazole-based dye should be fluorescent, as the open form is predominated at physiological pH. Thus, we envisioned that treatment of sensor **7** with HClO could provide a fluorescence turn-on signal under the physiological conditions.

As designed, the free sensor **7** is essentially nonfluorescent (Figure 7a). However, addition of HClO elicits a dramatic change in the fluorescence spectra. A significant fluorescence turn-on response was observed at 746 nm (extending into 870 nm). Mass, NMR, absorption, and emission spectrometry analysis confirmed that the fluorescence turn-on is indeed due to the HClO-mediated formation of the open form 1,3,4-oxadiazole-based fluorescent dye (Figures S18−21). In addition, as shown in Figure 7b, NIR sensor **7** is highly selective to HOCl over other various biologically relevant analytes (reactive oxygen species, reactive nitrogen species, and other relevant analytes.) represented by hydrogen peroxide (H_2O_2), superoxide ($O_2^{\bullet-}$), hydroxyl radical (OH·), *tert*-butyl hydroperoxide (TBHP), *tert*-butoxy radical (·O*t*Bu), nitric oxide (NO), NO_3^-, NO_2^-, ascorbic acid (AA), and dehydroascorbic acid (DHA), suggesting that the new NIR sensor is promising for applications in biological systems.

The new NIR sensor **7** was preliminarily applied to detect endogenously produced HClO in living macrophage cells. When stimulated by lipopolysaccharide (LPS) and phorbol myristate acetate (PMA), macrophages may produce endogenous HOCl.[26] The living RAW264.7 macrophage cells loaded with only NIR sensor **7** (5 μM) display almost no fluorescence (Figure 8a). However, after the macrophage cells have been incubated with LPS (1 μg/mL) for 12 h, and then further coincubated with PMA (1 μg/mL) and sensor **7** (5 μM) for 30 min, a dramatic enhancement in the NIR emission (Figure 8e) was observed. These data indicate that the new NIR sensor **7** is

Scheme 2. Synthesis of NIR Fluorescent Turn-on Sensor 7 for HOCl[a]

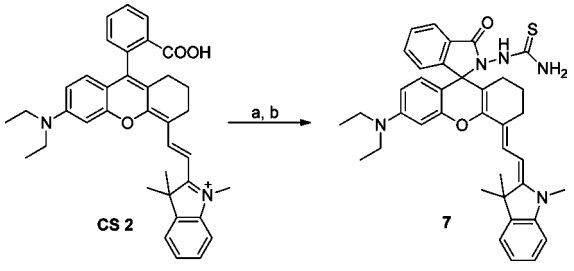

[a]Conditions: (a) *N*-hydroxysuccinimide (HOSu), DCC, CH_2Cl_2; (b) $NH_2NHCSNH_2$, TEA.

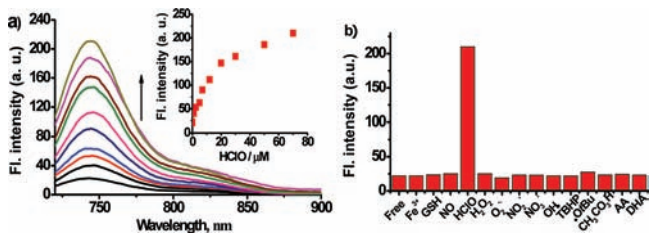

Figure 7. (a) Fluorescence spectra of NIR fluorescent sensor **7** (5 μM) in the presence of various concentrations of HClO (0−70 μM) in PBS buffer (50 mM, pH 7.4, containing 30% CH_3CN) with excitation at 690 nm. Inset: Fluorescence intensity of sensor **7** (5 μM) at 746 nm vs HClO concentration (0−70 μM). (b) The fluorescence intensity of sensor **7** at 746 nm excited at 690 nm in the presence of various biologically relevant analytes (70 μM).

dx.doi.org/10.1021/ja209292b | *J. Am. Chem.Soc.* 2012, 134, 1200−1211

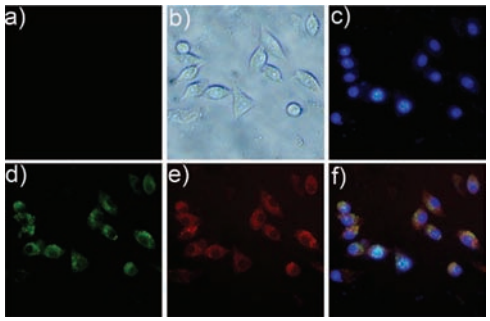

Figure 8. (a) Fluorescence image (red channel) of RAW264.7 macrophage cells incubated with only NIR sensor **7** (5 μM) for 60 min at 37 °C. (b–f) RAW264.7 macrophage cells pretreated with 1 μg/mL LPS for 12 h, further coincubated with PMA (1 μg/mL), sensor **7** (5 μM), Hoechst 33258 (4.5 μM), and Mito Tracker Green (5 μM) for 60 min. (b) DIC image; (c) emission from the blue channel (nuclear staining); (d) emission from the green channel (mitochondria staining); (e) emission from the red channel; and (f) overlay of the blue, green, and red channels.

capable of fluorescence imaging of endogenously produced HOCl in the living RAW264.7 macrophage cells. Notably, the nuclear staining with Hoechst 33258 (Figure 8c) suggests that the sensor has no obvious cytotoxicity to the cells. In addition, the nuclear staining (Figure 8c) and mitochondria staining (Figure 8d) reveal that sensor **7** associates with the mitochondria of RAW264.7 macrophage cells (Figure 3c–f).

The major advantage of the new NIR **CS** functional dyes over the traditional rhodamines is that our **CS** dyes have both absorption and emission in the NIR region while retaining the rhodamine-like fluorescence on–off switching mechanism by the spirocyclization. Thus, the unique NIR **CS** dyes are superior to the traditional rhodamines in that our **CS** dyes are favorable for biological imaging applications in living animals, as NIR light leads to minimum photodamage to biological samples, deep tissue penetration, and minimum interference from background autofluorescence by biomolecules in the living animals. Thus, we decided to examine the possibility of the new NIR sensor **7** for biological imaging of endogenously produced HClO in the living mice. The HClO production in vivo was generated by activated macrophages and neutrophils in an lipopolysaccharide (LPS) model of acute inflammation.[6] The ICR mice were divided into three groups. One group was untreated as the control group. The second group was given saline (400 μL) in the peritoneal cavity, followed by intraperitoneal (i.p.) injection with sensor **7** (120 nanomoles). The third group was given an i.p. injection of LPS (1 mg in 400 μL saline), and followed by i.p. injection with sensor **7** (120 nmol) after 4 h. The mice were anesthetized, and the abdominal fur was removed. Ten minutes after the sensor **7** injection, the mice were imaged using a FMT 2500 LX quantitative tomography in vivo imaging system. As shown in Figure 9c, the mice treated with both LPS and sensor **7** exhibited a significantly higher fluorescence readout (pseudocolor) than the untreated mice (Figure 9a) or mice treated with only sensor **7** (Figure 9b). The fluorescent intensity from the abdominal area of the mice was quantified, and the data indicate that the mice loaded with LPS and sensor **7** have approximately 4-fold higher fluorescence intensity than the mice loaded with saline and sensor **7** (Figure 9d). Thereby, these results demonstrate that the new NIR sensor **7** can image endogenously produced HClO in the living animals.

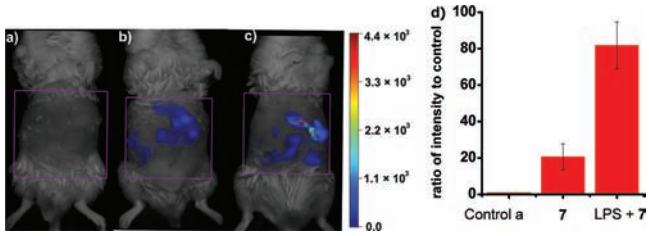

Figure 9. Representative fluorescent images (pseudocolor) of in vivo HClO production from the peritoneal cavity of the mice with sensor **7** during an LPS-mediated inflammatory response: (a) negative control, neither LPS nor sensor **7** was injected; (b) saline was injected in the intraperitoneal (i.p.) cavity of mice, followed by i.p. injection of sensor **7** (120 nmol); (c) LPS was injected into the peritoneal cavity of the mice, followed by i.p. injection of sensor **7** (120 nanomoles). Ten minutes after the sensor **7** injection, the mice were imaged using a FMT 2500 LX quantitative tomography in vivo imaging system with an excitation filter 670 nm and an emission range = 690–740 nm. (d) Quantification of fluorescence emission intensity from the groups a–c. The total number of photons from the entire peritoneal cavity of the groups a–c was integrated and plotted as a ratio to the control group a. The time-dependent and dose-dependent fluorescence images are shown in Figure S22.

■ CONCLUSION

In summary, we have introduced a new strategy to design NIR functional dyes with the carboxylic-acid-controlled fluorescence on–off switching mechanism by the spirocyclization. Based on the design strategy, we have synthesized a series of Changsha (**CS1–6**) NIR fluorophores, a unique class of NIR functional fluorescent dyes, bearing excellent photophysical properties while retaining the rhodamine-like fluorescence ON–OFF switching mechanism. Importantly, **CS1–6** NIR dyes are superior to the traditional rhodamine dyes with both absorption and emission in the NIR region. In addition, we have performed quantum chemical calculations with the B3LYP exchange functional employing 6-31G* basis sets using a suite of Gaussian 09 programs to provide insights into the structure-optical properties of **CS** NIR dyes. Furthermore, using **CS2** as a platform, we further constructed the novel NIR fluorescent TURN-ON sensor **7**, which is capable of imaging endogenously produced HClO in the living animals, demonstrating the value of our **CS** NIR functional fluorescent dyes. We expect that the design strategy may be extended for development of a wide variety of NIR functional dyes with a suitable fluorescence-controlled mechanism, and **CS1–6** will be employed as a molecular tool for numerous biological applications. Future efforts include development of ratiometric fluorescent sensors based on the **CS** NIR functional fluorescent dyes.

■ EXPERIMENTAL SECTION

Raw 264.7 Murine Macrophages Culture and Imaging Using Sensor 7. Raw 264.7 murine macrophages were obtained from Xiangya hospital and cultured in DMEM (Dulbecco's modified Eagle's medium) supplemented with 10% FBS (fetal bovine serum) in an atmosphere of 5% CO_2 and 95% air at 37 °C. For detection of endogenously produced HOCl, the living RAW 264.7 macrophages were treated with LPS (1 μg/mL) for 12 h and then further coincubated with PMA (1 μg/mL), sensor **7** (5 μM), Hoechst 33258 (4.5 μM), and Mito Tracker Green (5 μM) for 60 min. Prior to imaging, the cells were washed three times with 1 mL of PBS, and the fluorescence images were acquired through an Olympus fluorescence microscopy equipped with a cooled CCD camera.

Fluorescence Imaging in Living Mice. ICR mice (20–25 g) were given an intraperitoneal (i.p.) injection of LPS (1 mg in 400 μL

dx.doi.org/10.1021/ja209292b | J. Am. Chem.Soc. 2012, 134, 1200–1211

saline). After 4 h, the mice were anesthetized by an i.p. injection of xylazine (10 mg/kg) and ketamine (80 mg/kg) and the abdominal fur was removed with an electric shaver. Then, the mice were intraperitoneally injected with sensor **7** (400 μM in 400 μL of 1:3 = CH_3OH/PBS). As a control, untreated mice (neither treated with LPS nor sensor **7**) or unstimulated mice intraperitoneally injected only with sensor **7** (400 μM in 400 μL of 1:3 = CH_3OH/PBS) were also prepared. The mice were then imaged (10 min after the injection of sensor **7**) by using a FMT 2500 LX quantitative tomography in vivo imaging system, with an excitation filter of 670 nm and an emission filter of 690−740 nm.

Synthesis of Compounds CS 2−3, CS 5−6, and 5−6. Freshly distilled cyclohexanone (6.6 mL, 63.7 mmol) was added dropwise to concentrated H_2SO_4 (70 mL) and cooled down to 0 °C. Then, compound **1a**, **1b**, or **1c** (32 mmol) was added in portions with vigorous stirring. The reaction mixture was heated at 90 °C for 1.5 h, cooled down, and poured onto ice (300 g). Perchloric acid (70%; 7 mL) was then added, and the resulting precipitate was filtered off and washed with cold water (100 mL). Compound **2a**, **2b**, or **2c** obtained as a red solid was used for the next step without further purification.

Compound **2a**, **2b**, or **2c** (0.21 mmol) and Fisher aldehyde **3** or **4** (0.22 mmol) were dissolved in acetic anhydride (8 mL), and the reaction mixture was heated to 50 °C and further stirred at 50 °C for 30 min. Then, water (8 mL) was added to the reaction mixture to quench the reaction. The solvent was removed under reduced pressure to give the crude product, which was purified by silica gel flash chromatography using CH_2Cl_2 to CH_2Cl_2/ethanol (200:1 to 20:1) as eluent to afford compounds **CS 2−3** and **CS 5−6** as green solid and compounds **5−6** as blue solid.

CS 2. ^{1}H NMR (400 MHz, CD_3OD): 1.24 (t, J = 6.8 Hz, 6H), 1.81 (8H), 2.26−2.36 (m, 2H), 2.68 (t, J = 6.0 Hz, 2H), 3.52−3.57 (q, 4H), 3.63 (s, 3H), 6.16−6.19 (d, J = 13.6 Hz, 1H), 6.73−6.80 (3H), 7.26−7.32 (3H), 7.42 (t, J = 7.6 Hz, 1H), 7.54 (d, J = 7.2 Hz, 1H), 7.65−7.69 (td, J = 7.6, 1.2 Hz, 1H), 7.75−7.79 (td, J = 7.6, 1.2 Hz, 1H), 8.24 (d, J = 7, 2 Hz, 1H), 8.66−8.69 (d, J = 14.0 Hz, 1H). ^{13}C NMR (100 MHz, CD_3OD): 13.73, 26.19, 28.81, 29.63, 29.64, 32.66, 47.07, 51.49, 97.79, 101.55, 112.84, 114.54, 117.57, 124.37, 127.27, 130.28, 130.79, 131.46, 131.72, 132.43, 133.35, 135.12, 138.35, 143.29, 144.42, 145.33, 158.25, 165.46, 169.60. 176.22. MS (ESI) m/z 559.2 $(M\text{-}ClO_4)^+$; HRMS (ESI) m/z calcd for $C_{37}H_{39}N_2O_3^+$ $(M\text{-}ClO_4)^+$: 559.2955. Found 559.2967.

CS 3. ^{1}H NMR (500 MHz, CD_3OD):1.79−1.83 (8H), 1.89−1.92 (m, 2H), 2.14−2.17 (m, 2H), 2.31−2.34 (m, 2H), 2.62 (t, J = 6.0 Hz, 2H), 2.67 (s, 2H), 3.13 (t, J = 6.0 Hz, 2H), 3.41 (t, J = 5.8 Hz, 2H), 3.48 (t, J = 5.6 Hz, 2H), 3.56 (s, 3H), 6.02−6.05 (d, J = 13.6 Hz, 1H), 6.39 (s, 1H), 7.18−7.22 (3H), 7.38 (t, J = 7.6 Hz, 1H), 7.48 (d, J = 6.8 Hz, 1H), 7.64 (td, J = 7.6, 1.2 Hz, 1H), 7.73 (d, J = 7.6 Hz, 1H), 8.19 (dd, J = 7.0, 1.2 Hz, 1H), 8.59−8.62 (d, J = 13.6 Hz, 1H). ^{13}C NMR (100 MHz, $CDCl_3$): 22.13, 22.85, 23.01, 26.12, 26.16, 29.73, 29.78, 29.83, 31.72, 36.32, 51.74, 52.30, 99.46, 106.78, 111.92, 116.39, 118.16, 122.27, 124.23, 125.69, 126.20, 126.47, 130.68, 131.32, 133.01, 134.25, 137.95, 141.42, 142.76, 145.65, 150.71, 153.91, 164.98, 173.37. MS (ESI) m/z 583.3$(M\text{-}ClO_4)^+$; HRMS (ESI) m/z calcd for $C_{39}H_{39}N_2O_3^+$ $(M\text{-}ClO_4)^+$: 583.2955. Found 583.2969.

CS 5. ^{1}H NMR (400 MHz, CD_3OD): 1.23 (t, J = 6.8 Hz, 6H), 1.74−1.80 (m, 2H), 2.02 (6H), 2.42−2.60 (m, 2H), 2.65 (t, J = 6.0 Hz, 2H), 3.49−3.56 (q, 4H), 3.72 (s, 3H), 6.14−6.18 (d, J = 14.0 Hz, 1H), 6.65−6.73 (3H), 7.20−7.22 (d, J = 7.2 Hz, 1H), 7.43 (t, J = 7.6 Hz, 1H), 7.54−7.61 (3H), 7.69−7.739 (td, J = 7.6, 1.2 Hz, 1H), 7.93−7.98 (2H), 8.17 (d, J = 8.0 Hz, 1H), 8.26 (d, J = 8.4 Hz, 1H), 8.70−8.74 (d, J = 14.8 Hz, 1H). ^{13}C NMR (125 MHz, CD_3OD): 13.80, 22.69, 26.29, 28.86, 29.21, 31.74, 33.09, 46.93, 97.85, 101.46, 112.99, 114.22, 115.60, 117.32, 122.98, 124.49, 127.15, 129.79, 130.22, 130.39, 131.42, 131.76, 132.12, 132.75, 133.35, 134.53, 135.07, 135.92, 138.44, 142.69, 143.81, 154.38, 158.27, 165.21, 169.77, 177.89. MS (ESI) m/z 609.3 $(M\text{-}ClO_4)^+$; HRMS (ESI) m/z calcd for $C_{41}H_{41}N_2O_3^+$ $(M\text{-}ClO_4)^+$: 609.3112. Found 609.3125.

CS 6. ^{1}H NMR (500 MHz, CD_3OD):1.80−1.86 (m, 2H), 1.90−1.95 (m, 2H), 2.08 (s, 6H), 2.17−2.22 (m, 2H), 2.32−2.35 (t, J = 6.0 Hz, 2H), 2.62−2.65 (t, J = 6.0 Hz, 2H), 2.69−2.72 (t, J = 6.0 Hz, 2H), 3.17−3.20 (t, J = 6.0 Hz, 2H), 3.40−3.43 (t, J = 5.6 Hz, 2H), 3.46−3.50 (2H), 3.68 (s, 3H), 6.07−6.10 (d, J = 14.0 Hz, 1H), 6.39 (s, 1H), 7.21 (d, J = 7.6 Hz, 1H), 7.44 (t, J = 7.6 Hz, 1H), 7.55 (d, J = 8.8 Hz, 1H), 7.60−7.66 (2H), 7.72 (t, J = 7.6 Hz, 1H), 7.97 (t, J = 8.4 Hz, 2H), 8.19 (d, J = 8.0 Hz, 1H), 8.24 (d, J = 8.4 Hz, 1H), 8.70−8.74 (d, J = 14.0 Hz, 1H). ^{13}C NMR (125 MHz, $CDCl_3$): 21.89, 22.08, 25.17, 27.65, 28.44, 28.49, 28.74, 30.74, 31.72, 50.79, 51.31, 51.78, 98.65, 106.03, 111.68, 115.16, 116.89, 123.26, 124.50, 125.22, 125.66, 128.67, 129.55, 130.44, 130.67, 131.13, 131.64, 132.28, 133.18, 133.89, 140.50, 163.85. MS (ESI) m/z 633.3 $(M\text{-}ClO_4)^+$; HRMS (ESI) m/z calcd for $C_{43}H_{41}N_2O_3^+$ $(M\text{-}ClO_4)^+$: 633.3112. Found 633.3135.

5. ^{1}H NMR (500 MHz, $CDCl_3$):1.14−1.19 (3H), 1.73 (9H), 1.80−1.82 (3H), 2.02−2.10 (4H), 2.52 (1H), 2.64 (1H), 3.31−3.41 (4H), 4.02 (m, 1H), 5.57 (t, J = 14.4 Hz, 1H), 6.63 (t, J = 2.4 Hz, 1H), 6.76 (t, J = 8.4 Hz, 1H), 6.95−6.99 (2H), 7.20−7.26 (3H), 7.59 (t, J = 7.4 Hz, 1H), 7.66 (d, J = 7.6 Hz, 1H), 7.73 (t, J = 14.4 Hz, 1H), 8.04−8.07 (1H). ^{13}C NMR (100 MHz, $CDCl_3$): 13.11, 17.25, 21.29, 22.44, 27.98, 28.59, 30.76, 32.81, 44.59, 105.46, 113.77, 116.55, 117.32, 123.63, 124.74, 128.38, 128.46, 130.06, 130.14, 130.32, 131.27, 131.56, 134.07, 135.34, 143.48, 143.76, 144.58, 147.54, 152.41, 162.45, 172.35, 179.84. MS (ESI) m/z 587.3$(M\text{-}ClO_4)^+$; HRMS (ESI) m/z calcd for $C_{38}H_{39}N_2O_4^+$ $(M\text{-}ClO_4)^+$: 587.2904. Found 587.2917.

6. ^{1}H NMR (400 MHz, $CDCl_3$): 1.16−1.22 (3H), 1.70−1.79 (m, 3H), 1.82−1.84 (3H), 2.06−2.07 (10H), 2.50−2.70 (2H), 3.33−3.42 (m, 1H), 3.46−3.48 (3H), 4.01−4.10 (m, 1H), 5.67 (t, J = 14.4 Hz, 1H), 6.66 (d, J = 4.0 Hz, 1H), 7.01 (s, 1H), 7.16−7.22 (2H), 7.30−7.36 (m, 1H), 7.52−7.54 (m, 1H), 7.56 (t, J = 7.6 Hz, 1H), 7.64 (t, J = 7.6 Hz, 1H), 7.80−7.86 (2H), 7.94 (t, J = 14.4 Hz, Hz, 1H), 8.07−8.09 (1H), 7.14−8.16 (d, J = 8.4 Hz, 1H). ^{13}C NMR (100 MHz, $CDCl_3$): 12.96, 17.06, 19.19, 21.45, 22.64, 24.37, 24.77, 27.60, 27.69, 27.82, 30.56, 43.12, 109.50, 116.61, 118.09, 119.99, 121.87, 123.29, 124.73, 127.17, 128.74, 129.42, 129.96, 131.41, 133.82, 143.05, 150.02, 170.05. MS (ESI) m/z 637.3 $(M\text{-}ClO_4)^+$; HRMS (ESI) m/z calcd for $C_{42}H_{41}N_2O_4^+$ $(M\text{-}ClO_4)^+$: 637.3061. Found 637.3080.

Synthesis of Compounds CS 1 and CS 4. Compound **2a** (100.1 mg, 0.21 mmol) and Fisher aldehyde **3** or **4** (0.26 mmol) were dissolved in acetic anhydride (20 mL), and the reaction mixture were stirred at room temperature for 10 min. Then, the reaction mixture was poured into saturated $NaHCO_3$ solution (200 mL) and was extracted with CH_2Cl_2 (200 mL) for three times. The organic phases were combined and dried by anhydrous $MgSO_4$. The solution was then removed under reduced pressure to give the crude product, which was purified by silica gel flash chromatography using CH_2Cl_2 to CH_2Cl_2/ethanol (200:1 to 20:1) as eluent to afford compound **CS 1** or **CS 4** as a green solid.

CS 1. ^{1}H NMR (400 MHz, CD_3OD): 1.33 (3H), 1.78 (8H), 2.05 (s, 3H), 2.33 (2H), 2.67 (2H), 3.38 (2H), 3.56 (s, 3H), 6.07−6.10 (d, J = 14.0 Hz, 1H), 6.57 (s, 1H), 6.63−6.68 (m, 1H), 7.24 (3H), 7.40 (t, J = 7.2 Hz, 1H), 7.50 (t, J = 7.6 Hz, 1H), 7.66 (t, J = 7.2 Hz, 1H), 7.75 (t, J = 7.6 Hz, 1H), 8.22 (d, J = 7.2 Hz, 1H), 8.61 (1H). ^{13}C NMR (100 MHz, CD_3OD): 15.20, 18.60, 22.73, 26.25, 29.77, 32.38, 36.38, 40.13, 50.63, 95.50, 100.60, 112.41, 116.06, 117.66, 123.02, 124.28, 126.01, 126.76, 129.25, 130.73, 131.48, 133.24, 134.81, 138.17, 143.02, 143.14, 145.46, 154.96, 157.89, 165.53, 175.03. MS (ESI) m/z 545.3 $(M\text{-}ClO_4)^+$; HRMS (ESI) m/z calcd for $C_{36}H_{37}N_2O_3^+$ $(M\text{-}ClO_4)^+$: 545.2799. Found 545.2824.

CS 4. ^{1}H NMR (400 MHz, CD_3OD): 1.32 (t, J = 7.2 Hz, 3H), 1.80−1.84 (m, 2H), 2.05 (s, 3H), 2.07 (s, 3H), 2.08 (s, 3H), 2.30−2.35 (q, 2H), 2.69 (t, J = 5.6 Hz, 2H), 3.38−3.38 (m, 2H), 3.68 (s, 3H), 6.11−6.14 (d, J = 14.0 Hz, 1H), 6.55 (s, 1H), 6.69 (s, 1H), 7.23 (d, J = 7.6 Hz, 1H), 7.46 (t, J = 7.6 Hz, 1H), 7.56 (d, J = 9.2 Hz, 1H), 7.61−7.68 (2H), 7.75 (td, J = 6.8, 1.2 Hz, 1H), 7.98 (t, J = 8.8 Hz, 2H), 8.22 (d, J = 7.2 Hz, 1H), 8.31 (d, J = 8.4 Hz, 1H), 8.69−8.72 (d, J = 14.0 Hz, 1H). ^{13}C NMR (125 MHz, CD_3OD): 14.24, 17.56, 21.74, 25.31, 28.42, 31.65, 36.94, 39.19, 52.07, 94.69, 99.52, 111.78, 114.99, 116.40, 122.08, 123.42, 124.69, 125.88, 128.26, 128.70, 129.44, 130.36, 130.50, 131.07, 131.64, 132.14, 133.32, 133.57, 134.43, 137.16, 141.76, 153.77, 154.67, 156.77, 164.24, 175.89. MS (ESI) m/z 595.3 $(M\text{-}ClO_4)^+$; HRMS (ESI) m/z calcd for $C_{40}H_{39}N_2O_3^+$ $(M\text{-}ClO_4)^+$: 595.2955. Found 595.2963.

■ ASSOCIATED CONTENT

Supporting Information

Experimental procedures, some spectra, and complete ref 20. This material is available free of charge via the Internet at http://pubs.acs.org.

■ AUTHOR INFORMATION

Corresponding Author

weiyinglin@hnu.edu.cn

■ ACKNOWLEDGMENTS

Funding was partially provided by NSFC (20872032, 20972044, 21172063), NCET (08-0175), the Doctoral Fund of Chinese Ministry of Education (20100161110008), and the Fundamental Research Funds for the Central Universities, Hunan University.

■ REFERENCES

(1) For some reviews and some examples, see: (a) Loudet., A.; Burgess, K. *Chem. Rev.* **2007**, *107*, 4891−4932. (b) Goncalves., M. S. T. *Chem. Rev.* **2009**, *109*, 190−212. (c) Qian, X.; Xiao, Y.; Xu, Y.; Guo, X.; Qian, J.; Zhu, W. *Chem. Commun.* **2010**, *46*, 6418−6436. (d) Hapuarachchige, S.; Montano, G.; Ramesh, C.; Rodriguez, D.; Henson, L. H.; Williams, C. C.; Kadavakkollu, S.; Johnson, D. L.; Shuster, C. B.; Arterburn, J. B. *J. Am. Chem. Soc.* **2011**, *133*, 6780−6790. (e) Peng, X.; Yang, Z.; Wang, J.; Fan, J.; He, Y.; Song, F.; Wang, B.; Sun, S.; Qu, J.; Qi, J.; Yan, M. *J. Am. Chem. Soc.* **2011**, *133*, 6626−6635. (f) Sotgiu, G.; Galeotti, M.; Samor, C.; Bongini, A.; Mazzanti., A. *Chem.—Eur. J.* **2011**, *17*, 7947−7952. (g) Kim, E.; Koh, M.; Ryu, J.; Park, S. B. *J. Am. Chem. Soc.* **2008**, *130*, 12206−12207. (h) Peng, T.; Yang, D. *Org. Lett.* **2010**, *12*, 496−499. (i) Fischer, G. M.; Jüngst, C.; Isomaki-Krondahl, M.; Gauss, D.; Moller, H. M.; Daltrozzo, E.; Zumbusch, A. *Chem. Commun.* **2010**, *46*, 5289−5291. (j) Baumes, J. M.; Gassensmith, J. J.; Giblin, J.; Lee, J.-J.; White, A. G.; Culligan, W. J.; Leevy, W. M.; Kuno, M.; Smith, B. D. *Nat. Chem.* **2010**, *2*, 1025−1030. (k) Matsui, A.; Umezawa, K.; Shindo, Y.; Fujii, T.; Citterio, D.; Oka, K.; Suzuki, K. *Chem. Commun.* **2011**, *47*, 10407−10409. (l) Yang, Y.; Lowry, M.; Xu, X.; Escobedo, J. O.; Sibrian-Vazquez, M.; Wong, L.; Schowalter, C. M.; Jensen, T. J.; Fronczek, F. R.; Warner, I. M.; Strongin, R. M. *Proc. Natl. Acad. Sci. U.S.A.* **2008**, *105*, 8829−8834. (m) Kamiya, M.; Asanuma, D.; Kuranaga, E.; Takeishi, A.; Sakabe, M.; Miura, M.; Nagano, T.; Urano, Y. *J. Am. Chem. Soc.* **2011**, *133*, 12960−12963. (n) Dasari, M.; Lee, S.; Sy, J.; Kim, D.; Lee, S.; Brown, M.; Davis, M.; Murthy, N. *Org. Lett.* **2010**, *12*, 3300−3303. (o) Yu, Z.; L. Ho, Y.; Lin, Q. *J. Am. Chem. Soc.* **2011**, *133*, 11912−11925. (p) Ueno, T.; Nagano, T. *Nat. Methods* **2011**, *8*, 642−645.

(2) For some reviews, see: (a) de Silva, A. P.; Gunaratne, H. Q. N.; Gunnlaugsson, T.; Huxley, A. J. M.; McCoy, C. P.; Rademacher, J. T.; Rice, T. E. *Chem. Rev.* **1997**, *97*, 1515−1566. (b) Nolan, E. M.; Lippard, S. J. *Chem. Rev.* **2008**, *108*, 3443−3480. (c) Que, E. L.; Domaille, D. W.; Chang, C. J. *Chem. Rev.* **2008**, *108*, 1517−1549. (d) Quang, D. T.; Kim, J. S. *Chem. Rev.* **2010**, *110*, 6280−6301. (e) Thomas, S. W. III; Joly, G. D.; Swager, T. M. *Chem. Rev.* **2007**, *107*, 1339−1386. (f) Han, J.; Burgess, K. *Chem. Rev.* **2010**, *110*, 2709−2728. (g) Kobayashi, H.; Ogawa, M.; Alford, R.; Choyke, P. L.; Urano, Y. *Chem. Rev.* **2010**, *110*, 2620−2640. (h) Cho, D.-G.; Sessler, J. L. *Chem. Soc. Rev.* **2009**, *38*, 1647−1662. (i) Chen, X.; Zhou, Y.; Peng, X.; Yoon, J. *Chem. Soc. Rev.* **2010**, *39*, 2120−2135.

(3) For some reviews and examples, see: (a) Kiyose, K.; Kojima, H.; Nagano, T. *Chem. Asian J.* **2008**, *3*, 506−515. (b) Qian, G.; Wang, Z. Y. *Chem. Asian J.* **2010**, *5*, 1006−1029. (c) Weissleder, R. *Nat. Biotechnol.* **2001**, *19*, 316−317. (d) Kobayashi, H.; Longmire, M. R.; Ogawa, M.; Choyke, P. L. *Chem. Soc. Rev.* **2011**, *40*, 4626−4648. (e) Licha, K. *Top. Curr. Chem.* **2002**, *222*, 1−29. (f) Frangioni, J. V. *Curr. Opin. Chem. Biol.* **2003**, *7*, 626−634. (g) Escobedo, J. O.; Rusin, O.; Lim, S.; Strongin, R. M. *Curr. Opin. Chem. Biol.* **2010**, *14*, 64−70. (h) Hilderbrand, S. A.; Weissleder, R. *Curr. Opin. Chem. Biol.* **2010**, *14*, 71−79. (i) *Near-Infrared Applications in Biotechnology*; Raghavachari, R., Ed.; Marcel Dekker, New York, 2001. (j) Johnson, J. R.; Fu, N.; Arunkumar, E.; Leevy, W. M.; Gammon, S. T.; Piwnica-Worms, D.; Smith, B. D. *Angew. Chem., Int. Ed.* **2007**, *46*, 5528−5531.

(4) (a) Kiyose, K.; Aizawa, S.; Sasaki, E.; Kojima, H.; Hanaoka, K.; Terai, T.; Urano, Y.; Nagano, T. *Chem.—Eur. J.* **2009**, *15*, 9191−9200. (b) Egawa, T.; Hanaoka, K.; Koide, Y.; Ujita, S.; Takahashi, N.; Ikegaya, Y.; Matsuki, N.; Terai, T.; Ueno, T.; Komatsu, T.; Nagano, T. *J. Am. Chem. Soc.* **2011**, *133*, 14157−14159.

(5) For some examples, see: (a) Ozmen, B.; Akkaya, E. U. *Tetrahedron Lett.* **2000**, *41*, 9185−9188. (b) Sasaki, E.; Kojima, H.; Nishimatsu, H.; Urano, Y.; Kikuchi, K.; Hirata, Y.; Nagano, T. *J. Am. Chem. Soc.* **2005**, *127*, 3684−3685. (c) Tang, B.; Yu, F.; Li, P.; Tong, L.; Duan, X.; Xie, T.; Wang, X. *J. Am. Chem. Soc.* **2009**, *131*, 3016−3023. (d) Yu, F.; Li, P.; Li, G.; Zhao, G.-J.; Chu, T.-S.; Han, K.-L. *J. Am. Chem. Soc.* **2011**, *133*, 11030−11033.

(6) Kundu, K.; Knight, F.; Willett, N.; Lee, S.; Taylor, W. R.; Murthy, N. *Angew. Chem., Int. Ed.* **2009**, *48*, 299−303.

(7) Karton-Lifshin, N.; Segal, E.; Omer, L.; Portnoy, M.; Satchi-Fainaro, R.; Shabat, D. *J. Am. Chem. Soc.* **2011**, *133*, 10960−10965.

(8) For some reviews, see: (a) Kim, H. N.; Lee, M. H.; Kim, H. J.; Kim, J. S.; Yoon, J. *Chem. Soc. Rev.* **2008**, *37*, 1465−1472. (b) Beija, M.; Afonso, C. A. M.; Martinho, J. M. G. *Chem. Soc. Rev.* **2009**, *38*, 2410−2433. (c) Kubin, R. F.; Fletcher, A. N. *J. Lumin.* **1982**, *27*, 455−462.

(9) Dujols, V.; Ford, F.; Czarnik, A. W. *J. Am. Chem. Soc.* **1997**, *119*, 7386−7387.

(10) For some examples, see: (a) Chatterjee, A.; Santra, M.; Won, N.; Kim, S.; Kim, J. K.; Kim, S. B.; Ahn, K. H. *J. Am. Chem. Soc.* **2009**, *131*, 2040−2041. (b) Kwon, J. Y.; Jang, Y. J.; Lee, Y. J.; Kim, K.-M.; Seo, M.-S.; Nam, W.; Yoon, J. *J. Am. Chem. Soc.* **2005**, *127*, 10107−10111. (c) Jou, M. J.; Chen, X.; Swamy, K. M. K.; Kim, H. N.; Kim, H.-J.; Lee, S.-g.; Yoon, J. *Chem. Commun.* **2009**, 7218−7220. (d) Egorova, O. A.; Seo, H.; Chatterjee, A.; Ahn, K. H. *Org. Lett.* **2010**, *12*, 401−403. (e) Du, P.; Lippard, S. J. *Inorg. Chem.* **2010**, *49*, 10753−10755. (f) Yuan, L.; Lin, W.; Yang, Y.; Song, J. *Chem. Commun.* **2011**, *47*, 4703−4705. (g) Li, H.; Fan, J.; Song, F.; Zhu, H.; Du, J.; Sun, S.; Peng, X. *Chem.—Eur. J.* **2010**, *16*, 12349−12356. (h) Sasaki, H.; Hanaoka, K.; Urano, Y.; Terai, T.; Nagano, T. *Bioorg. Med. Chem.* **2011**, *19*, 1072−1078.

(11) (a) Abugo, O. O.; Nair, R.; Lakowicz, J. R. *Anal. Biochem.* **2000**, *279*, 142−150. (b) Lieberwirth, U.; Arden-Jacob, J.; Drexhage, K. H.; Herten, D. P.; Muller, R.; Neumann, M.; Schulz, A.; Siebert, S.; Sagner, G.; Klingel, S.; Sauer, M.; Wolfrum, J. *Anal. Chem.* **1998**, *70*, 4771−4779.

(12) (a) Fu, M.; Xiao, Y.; Qian, X.; Zhao, D.; Xu, Y. *Chem. Commun.* **2008**, *15*, 1780−1782. (b) Koide, Y.; Urano, Y.; Hanaoka, K.; Terai, T.; Nagano, T. *J. Am. Chem. Soc.* **2011**, *133*, 5680−5682.

(13) Czerney, P.; Grummt, U.-W.; *J. Chem. Res., Synop.* **1996**, *4*, 173; Inst. Phys. Chem., Friedrich-Schiller-Univ., D-07743 Jena, Germany; EN.

(14) Lin, Y.; Weissleder, R.; Tung, C.-H. *Bioconjugate Chem.* **2002**, *13*, 605−610.

(15) (a) Shoda, T.; Kikuchi, K.; Kojima, H.; Urano, Y.; Komatsu, H.; Suzuki, K.; Nagano, T. *Analyst* **2003**, *128*, 719−723. (b) Liu, Q.-H.; Yan, X.-L.; Guo, J.-C.; Wang, D.-H.; Li, L.; Yan, F.-Y.; Chen, L.-G. *Spectrochim. Acta, Part A* **2009**, *73*, 789−793.

(16) Wang, J.; Cao, W.-F.; Su, J.-H.; Tian, H.; Huang, Y.-H.; Sun, Z.-R. *Dyes Pigm.* **2003**, *57*, 171−179.

(17) Oushiki, D.; Kojima, H.; Terai, T.; Arita, M.; Hanaoka, K.; Urano, Y.; Nagano, T. *J. Am. Chem. Soc.* **2010**, *132*, 2795−2801.

(18) Valeur, B. *Molecular Fluorescence: Principles and Applications*; Wiley-VCH: Weinheim, 2001.

(19) For some examples, see: (a) Lavis, L. D.; Chao, T.-Y.; Raines, R. T. *ACS Chem. Biol.* **2006**, *1*, 252−260. (b) Chandran, S. S.; Dickson, K. A.; Raines, R. T. *J. Am. Chem. Soc.* **2005**, *127*, 1652−1653. (c) Li, J.; Yao, S. Q. *Org. Lett.* **2009**, *11*, 405−408. (d) Peng, T.; Yang, D. *Org. Lett.* **2010**, *12*, 4932−4935.

(20) Frisch, M. J. et al. *GAUSSIAN 09* (Revision A.02), Gaussian, Inc.: Pittsburgh, PA, 2009.
(21) Urano, Y.; Kamiya, M.; Kanda, K.; Ueno, T.; Hirose, K.; Nagano, T. *J. Am. Chem. Soc.* **2005**, *127*, 4888−4894.
(22) (a) Bouit, P.-A.; Aronica, C.; Toupet, L.; Guennic, B. L.; Andraud, C.; Maury, O. *J. Am. Chem. Soc.* **2010**, *132*, 4328−4335. (b) Ohira, S.; Hales, J. M.; Thorley, K. J.; Anderson, H. L.; Perry, J. W.; Brédas, J.-L. *J. Am. Chem. Soc.* **2009**, *131*, 6099−6101. (c) Wrthner, F.; Archetti, G.; Schmidt, R.; Kuball, H.-G. *Angew. Chem., Int. Ed.* **2008**, *47*, 4529−4532.
(23) (a) Hidalgo, E.; Bartolome., R.; Dominguez, C. *Chem.-Biol. Interact.* **2002**, *139*, 265−282. (b) O'Brien, P. J. *Chem.-Biol. Interact.* **2000**, *129*, 113−139. (c) Harrison, J. E.; Schultz, J. *J. Biol. Chem.* **1976**, *251*, 1371−1374. (d) Lambeth, J. D. *Free Radical Biol. Med.* **2007**, *43*, 332−347.
(24) (a) Daugherty, A.; Dunn, J. L.; Rateri., D. L.; Heinecke, J. W. *J. Clin. Invest.* **1994**, *94*, 437−444. (b) Jenner, A. M.; Ruiz, J. E.; Dunster, C.; Halliwell, B.; Mann, G. E.; Siow, R. C. M. *Arterioscler., Thromb., Vasc. Biol.* **2002**, *22*, 574−580. (c) Huang, K. C.; Yang, C. C.; Lee, K. T.; Chien, C. T. *Kidney Int.* **2003**, *64*, 704−714. (d) Zavodnik, I. B.; Lapshina, E. A.; Zavodnik, L. B.; Soszyński, M.; Bartosz, G.; Bryszewska, M. *Bioelectrochemistry* **2002**, *58*, 127−135. (e) Hammerschmidt, S.; Büchler, N.; Wahn, H. *Chest* **2002**, *121*, 573−581. (f) Wu, S .M.; Pizzo, S. V. *Arch. Biochem. Biophys.* **2001**, *391*, 119−126. (g) Weitzman, S. A.; Gordon, L. I. *Blood* **1990**, *76*, 655−663.
(25) (a) Hiremath, S. P.; Biradir, J. S.; Kudari, S. M. *J. Ind. Chem. Soc.* **1984**, *61*, 74−76. (b) Amir, M.; Kumar, S. *Ind. J. Heterocycl .Chem.* **2004**, *14*, 51−54. (c) Amir, M.; Khan, M. S. Y.; Zaman, M. S. *Indian J. Chem., Sect. B* **2004**, *43B*, 2189−2194. (d) Shinde, A. D.; Kale, B. Y.; Shingate, B. B.; Shingare, M. S. *J. Korean Chem. Soc.* **2010**, *54*, 582−588. (e) Palaska, E.; Sahin, G.; Kelicen, P.; Durlu, N. T.; Altinok, G. *Il Farmaco.* **2002**, *57*, 101−107. (f) Rivera, N. R.; Balsells, J.; Hansen, K. B. *Tetrahedron Lett.* **2006**, *47*, 4889−4891. (g) Golovlyova, S. M.; Moskvichev, Y. A.; Alov, E. M.; Kobylinsky, D. B.; Ermolaeva, V. V. *Chem. Heterocycl. Compd.* **2001**, *37*, 1102−1106.
(26) (a) Adachi, Y.; Kindzelskii, A. L.; Petty, A. R.; Huang, J. B.; Maeda, N.; Yotsumoto, S.; Aratani, Y.; Ohno, N.; Petty, H. R. *J. Immunol.* **2006**, *176*, 5033−5040. (b) Gomez-Mejiba, S. E.; Zhai, Z.; Gimenez, M. S.; Ashby, M. T.; Chilakapati, J; Kitchin, K.; Mason, R. P.; Ramirez, D. C. *J. Biol. Chem.* **2010**, *285*, 20062−20071. (c) Test, S. T.; Weiss, S. J. *Adv. Free Radical Biol. Med.* **1986**, *2*, 91−116. (d) Bergt, C.; Marsche, G.; Panzenboeck, U.; Heinecke, J. W.; Malle, E.; Sattler, W. *Eur. J. Biochem.* **2001**, *268*, 3523−3531.